Journal of Engineering Mathematics **50:** 141–156, 2004.

Flow of surfactant-laden thin films down an inclined plane

B.D. EDMONSTONE, O.K. MATAR and R.V. CRASTER[1]
Department of Chemical Engineering and Chemical Technology, Imperial College London, South Kensington, London, SW7 2AZ, UK (o.matar@imperial.ac.uk); [1]Department of Mathematics, Imperial College London, South Kensington, London, SW7 2AZ, UK

Received 15 December 2003; accepted in revised form 21 July 2004

Abstract. A theory is formulated to describe the dynamics of a thin film flowing down an inclined plane laden with insoluble surfactant, present in dilute concentrations. Use of lubrication theory yields a coupled pair of partial differential equations for the film height and surfactant monolayer concentration. The contact line singularity is relieved by assuming the presence of a thin precursor layer ahead of the advancing film. Base flow solutions for a flow of constant flux are examined over various inclination angle, precursor-layer thickness, Peclet number, and capillary parameter ranges. Application of a transient growth analysis highlights the presence of an instability and the vulnerability of the flow to transverse disturbances of intermediate wavenumber. Our results reveal that several key features of the much-studied uncontaminated film flow, including stability, are modified qualitatively by the inclusion of surfactant.

Key words: interfacial instability, lubrication, surfactant, thin films

1. Introduction

Thin liquid films appear across a wide range of contexts, spanning engineering, manufacturing and biophysics. Their applications are relevant not only to chemical engineering and materials processing, but also to numerous biological processes, many of which are found within mammalian systems [1]. In many of these settings an advancing fluid front is susceptible to a transverse instability which can lead to rivulet formation, in the form of slender or triangular saw-tooth fingers, which is undesirable in applications such as coating-flow technology. In the presence of surfactant, and hence Marangoni driving forces, another instability resulting in the formation of fingering patterns is also known to occur (see [2–4] and references therein).

Interest in coating flows developed from experimental work which highlighted the existence of rivulet formation originating at the thickened front, located at the film's leading edge [5, 6]. These experimental observations were complemented by modelling work which proposed mechanisms for fingering at the gravitationally driven fluid front, [7–9]. Further experimental studies [10] produced detailed images of the fingering structures formed for varying inclination angles. More recent work has returned to modelling of the problem with observations of steady-state finger formation [11–13], and methods proposed for controlling the front instability, driving it into predetermined or controlled pattern formation [14, 15].

The majority of the studies mentioned above, however, have involved uncontaminated liquid films. With the addition of a surfactant into the problem, solutocapillary flow must be taken into account. The flows generated by solutocapillarity are mainly of interest in biological systems such as membranes, linings, and tear films, but they also appear within some manufacturing techniques [16]. Of particular interest are the effects of Marangoni flow on the front dynamics, flow stability, and surfactant transport. The majority of the research involving

surfactant-driven flows has been conducted in connection with surfactant-replacement therapy (SRT), a treatment for both neonate and adult respiratory distress syndrome. This subject has been covered extensively by previous investigators who have examined the steady-state [17], dynamic spreading of insoluble, [18–20], and soluble surfactants [21,22], and the process of surfactant-enhanced drug delivery [23,24]. The stability of the spreading process, which is often accompanied by fingering phenomena has also received considerable attention [2–4], [25–28].

In this paper, we investigate a gravitationally driven flow in the presence of a dilute surfactant. Evolution equations for the film thickness and surfactant monolayer concentration are derived using lubrication theory and applied to a flow with constant flux; a precursor layer model is used to relieve the contact line singularity. The effects of gravity, Marangoni stress, inclination angle, precursor layer thickness, capillarity, and surface diffusion on the flow are considered, while van der Waals, and inertial forces are neglected [25]. In addition to the base state height and surfactant concentration profiles, the stability of the flow is examined using suitable transient growth measures over a wide range of conditions. Our results reveal how the presence of surfactant modifies the instability which exists at the advancing front of an uncontaminated gravitationally driven thin film.

The rest of the paper is structured as follows. Section 2 details the problem formulation. Section 3 focuses on a discussion of the numerical results, while Section 4 contains some concluding remarks.

2. Mathematical formulation

We consider a thin layer of an incompressible, Newtonian fluid of constant viscosity μ, and density ρ, lying on an inclined plane bounded from below by a rigid, impermeable solid substrate and from above by an inviscid gas; this is shown schematically in Figure 1. The film is partially covered with insoluble surfactant of initially uniform concentration, Γ_m, which is assumed to be much smaller than the saturation concentration. We assume that the film flows out of a reservoir at the flow origin which provides a constant flux of fluid and surfactant.

The liquid–air boundary is a deformable interface located at $z = h(x, y, t)$, where x, y and z are the streamwise, transverse and surface normal coordinates, respectively, while t denotes time. The characteristic depth of the film, H, is considered to be small in comparison to the lateral extent of the film L: $\epsilon = H/L \ll 1$; in such a situation lubrication theory can be applied.

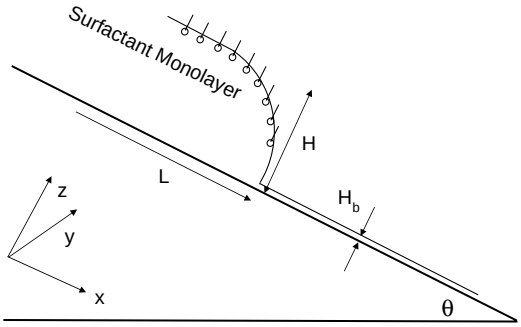

Figure 1. Schematic representation of the flow configuration for a thin film lying on an inclined pre-wetted substrate partially covered with surfactant.

Note that the film spreads over a pre-wetted solid substrate, which is covered by a precursor layer of uniform thickness H_b [7].

The governing equations are non-dimensionalized as follows, where overbars denote dimensionless quantities: $x = L\bar{x}$, $y = L\bar{y}$, $z = H\bar{z}$, $u = U\bar{u}$, $v = U\bar{v}$, $w = \epsilon U\bar{w}$, $t = (\mu L^2/\Pi H)\bar{t}$, $p = (\Pi/H)\bar{p}$, $\bar{\sigma} = (\sigma - \sigma_m)/\Pi$, $\Gamma = \Gamma_m\bar{\Gamma}$, where u, v, w, p, denote the streamwise, transverse, and normal components of the velocity field, **u**, and pressure, respectively. Here, $\Pi = \sigma_o - \sigma_m$, the spreading pressure, is the difference between the maximal and initial values of the surface tension, σ_o and σ_m, respectively, and is used to scale the local surface tension, σ. Finally, $U = \Pi H/\mu L$ is the characteristic Marangoni velocity in this problem. The overbars are henceforth suppressed and the equations in the following section are written in dimensionless variables, unless otherwise stated.

2.1. Hydrodynamics

Substitution of the above scalings in the governing mass and momentum equations yields, in the lubrication approximation,

$$u_x + v_y + w_z = 0, \tag{1}$$

$$p_x - u_{zz} - G\sin\theta = 0, \tag{2}$$

$$p_y - v_{zz} = 0, \tag{3}$$

$$p_z = 0, \tag{4}$$

where subscripts denote partial differentiation with respect to that coordinate and $G \equiv \rho g H L/\Pi$ is a Bond number. The tangential and normal stress balances at the film surface, $z = h(x, y, t)$, are given by,

$$u_z = \sigma_x, \tag{5}$$

$$v_z = \sigma_y, \tag{6}$$

$$p = -C\nabla^2 h, \tag{7}$$

where, $C \equiv \epsilon^2\sigma_m/\Pi$ is a capillary parameter. Although capillary forces scale as ϵ^2, the associated terms will be retained due to their regularizing effect. The kinematic boundary condition is given by,

$$h_t + \left(\int_0^h u\,\mathrm{d}z\right)_x + \left(\int_0^h v\,\mathrm{d}z\right)_y = 0. \tag{8}$$

For closure, a linear surfactant equation of state is chosen, which in dimensional form, is given by,

$$\sigma(\Gamma) = \sigma_o - \alpha_\Gamma\Gamma, \tag{9}$$

where, $\alpha_\Gamma = -(\partial\sigma/\partial\Gamma)_{\Gamma=0}$. In dimensionless form, this equation is expressed by

$$\sigma = 1 - \Gamma. \tag{10}$$

Integration of (2–4), application of no slip and no penetration conditions ($u = w = 0$ at $z = 0$) and use of (5), (6) and (10) results in,

$$u = \tfrac{1}{2}z(z - 2h)(p_x - G\sin\theta) - z\Gamma_x, \tag{11}$$

$$v = \tfrac{1}{2}z(z - 2h)p_y - z\Gamma_y. \tag{12}$$

Substitution of Equation (7) in (11) and (12) and substitution of the resultant solutions in Equation (8) yields the following film height evolution equation,

$$h_t = \nabla \cdot \left[\frac{h^3}{3}(-C\nabla\nabla^2 h) + \frac{h^2}{2}\nabla\Gamma \right] - \left[\frac{h^3}{3} G \sin\theta \right]_x . \tag{13}$$

The leading-order dimensionless equation of surfactant mass conservation is,

$$\Gamma_t + \nabla \cdot (\mathbf{u}_s \Gamma) = \frac{\nabla^2 \Gamma}{\mathrm{Pe}}, \tag{14}$$

where the subscript 's' denotes quantities evaluated at $z = h(x, y, t)$. For Equation (14) the surface velocity, $\mathbf{u}_s$, is given by,

$$\mathbf{u}_s = \frac{h^2}{2}\left[C\nabla\nabla^2 h + G\sin\theta \right] - h\nabla\Gamma, \tag{15}$$

while, $\mathrm{Pe} \equiv \Pi H/\mu D_s$, is a surface Peclet number, with D_s representing the surface diffusivity of the surfactant.

Substitution of Equation (15) in Equation (14) yields the relevant surfactant monolayer evolution equation,

$$\Gamma_t = \frac{\nabla^2\Gamma}{\mathrm{Pe}} + \nabla \cdot \left[-\frac{h^2}{2}\Gamma C\nabla\nabla^2 h + h\Gamma\nabla\Gamma \right] - \left[\frac{h^2}{2}\Gamma G\sin\theta \right]_x . \tag{16}$$

Note that (13) and (16) are further parameterized by another dimensionless group, $b \equiv H_b/H$, which is a ratio of the precursor thickness to the characteristic film thickness.

2.2. Travelling-wave solutions

The one-dimensional (1-D) forms of (13) and (16) are given by,

$$h_t = \left[-\frac{h^3}{3} C h_{xxx} + \frac{h^2}{2}\Gamma_x - \frac{h^3}{3} G\sin\theta \right]_x , \tag{17}$$

$$\Gamma_t = \frac{\Gamma_{xx}}{\mathrm{Pe}} + \left[\frac{h^2}{2}\Gamma(-Ch_{xxx}) + h\Gamma\Gamma_x - \frac{h^2}{2}\Gamma G\sin\theta \right]_x . \tag{18}$$

Given that flow down an inclined plane in the absence of surfactant gives rise to travelling-wave (TW) solutions, we postulate the existence of such solutions in the present problem and move into a frame of reference travelling with the wave:

$$\xi = x - ct, \quad h(x,t) = \mathbb{H}(\xi), \quad \Gamma(x,t) = \mathbb{G}(\xi), \tag{19}$$

where c is the speed of the TW so that the above equations in the limit of $\mathrm{Pe} \to \infty$ become

$$\left[c\mathbb{H} - \frac{\mathbb{H}^3}{3} C\mathbb{H}_{\xi\xi\xi} + \frac{\mathbb{H}^2}{2}\mathbb{G}_\xi - \frac{\mathbb{H}^3}{3} G\sin\theta \right]_\xi = 0, \tag{20}$$

$$\left[c\mathbb{G} - \frac{\mathbb{H}^2}{2}\mathbb{G}C\mathbb{H}_{\xi\xi\xi} + \mathbb{H}\mathbb{G}\mathbb{G}_\xi - \frac{\mathbb{H}^2}{2}\mathbb{G}G\sin\theta \right]_\xi = 0. \tag{21}$$

Integrating (20) and (21) from $-\infty$ to ∞ with the following boundary conditions

$$\xi \to \infty, \quad \mathbb{H} \to b, \quad \mathbb{H}_{\xi\xi\xi} \to 0, \quad \mathbb{G} \to 0, \quad \mathbb{G}_\xi \to 0, \tag{22}$$

$$\xi \to -\infty, \quad \mathbb{H} \to 1, \quad \mathbb{H}_{\xi\xi\xi} \to 0, \quad \mathbb{G} \to 1, \quad \mathbb{G}_\xi \to 0, \tag{23}$$

yields the following relations for c:

$$c = \frac{(1-b^3)}{3(1-b)} G \sin\theta, \tag{24}$$

$$c = \frac{G}{2} \sin\theta. \tag{25}$$

Equations (24) and (25) give different values for c, unless b takes the unique value of 0·366, which is too large to be of interest here. Hence there are no steady travelling-wave solutions for both (17) and (18). In general, the front propagation will be controlled by the smaller velocity proposed by (24), as seen in the numerical solutions to be discussed below.

In order to investigate any structural changes in the flow introduced by the inclusion of surfactant (for example the "step" structure that will be discussed later), Equations (20) and (21) can be integrated from $\xi_s - \delta$ to $\xi_s + \delta$, where δ is a very small distance from the location of the step, ξ_s; the following boundary conditions should be used:

$$\xi > \xi_s, \quad \mathbb{H} = b, \quad \mathbb{H}_{\xi\xi\xi} = 0, \quad \mathbb{G} = 0, \quad \mathbb{G}_\xi = 0, \tag{26}$$

$$\xi < \xi_s, \quad \mathbb{H} \equiv \mathbb{H}_0, \quad \mathbb{H}_{\xi\xi\xi} = 0, \quad \mathbb{G} \equiv \mathbb{G}_0, \quad \mathbb{G}_\xi \equiv -\tau, \tag{27}$$

where $\mathbb{H}_0$, $\mathbb{G}_0$ and τ represent the height of the step, the concentration and concentration gradient in that region, respectively. Integration of (20) and (21) subject to these boundary conditions yields

$$cb - \frac{b^3}{3} G \sin\theta - c\mathbb{H}_0 + \frac{\tau}{2}\mathbb{H}_0^2 + \frac{\mathbb{H}_0^3}{3} G \sin\theta = 0, \tag{28}$$

$$\mathbb{G}_0 \left(c - \mathbb{H}_0 \tau - \frac{\mathbb{H}_0^2}{2} G \sin\theta \right) = 0, \tag{29}$$

from which

$$\tau = \frac{c}{\mathbb{H}_0} - \frac{\mathbb{H}_0}{2} G \sin\theta, \tag{30}$$

$$c\left(b - \frac{\mathbb{H}_0}{2}\right) + \frac{G\sin\theta}{3}\left(\frac{\mathbb{H}_0^3}{4} - b^3\right) = 0. \tag{31}$$

Equation (31) should be solved to find $\mathbb{H}_0$; here c is given by (24). Note that if the second term in (31) is neglected, then $\mathbb{H}_0 = 2b$ (which appears to be the case in our computations, shown later; see the inset in Figure 6(e)). If, however, $c = 0$ then $\mathbb{H}_0 = 4^{1/3} b$. Importantly, we note that later numerical simulations show that the travelling fronts do indeed progress at uniform velocity, however, the surfactant concentration grows with time at the capillary ridge; the analysis above ignores this. Nonetheless, the value of c, and step height are confirmed by numerical simulations.

2.3. Transient growth

We examine the flow stability by decomposing the flow into its (1-D) base states, $(h^{(0)}, \Gamma^{(0)})(x,t)$ and applied infinitesimal disturbances, $(h^{(1)}, \Gamma^{(1)})(x,t)e^{iky}$:

$$h_t^{(0)} = \left[\frac{h^{(0)3}}{3}(-Ch_{xxx}^{(0)}) + \frac{h^{(0)2}}{2}\Gamma_x^{(0)} - \frac{h^{(0)3}}{3}G\sin\theta \right]_x, \tag{32}$$

$$\Gamma_t^{(0)} = \frac{\Gamma_{xx}^{(0)}}{\mathrm{Pe}} + \left[\frac{h^{(0)2}}{2}\Gamma^{(0)}(-Ch_{xxx}^{(0)}) + h^{(0)}\Gamma^{(0)}\Gamma_x^{(0)} - \frac{h^{(0)2}}{2}\Gamma^{(0)}G\sin\theta \right]_x, \tag{33}$$

$$\begin{aligned} h_t^{(1)} = {} & \left[\frac{h^{(0)3}}{3}(-Ch_{xxx}^{(1)}) + h^{(0)2}h^{(1)}(-Ch_{xxx}^{(0)}) + \frac{h^{(0)3}}{3}(Ch_x^{(1)}k^2) + \frac{h^{(0)2}}{2}\Gamma_x^{(1)} \right. \\ & \left. + h^{(0)}h^{(1)}\Gamma_x^{(0)} - h^{(0)2}h^{(1)}G\sin\theta \right]_x - \frac{h^{(0)3}}{3}Ch^{(1)}k^4 + \frac{h^{(0)3}}{3}Ch_{xx}^{(1)}k^2 \\ & - \frac{h^{(0)2}}{2}\Gamma^{(1)}k^2, \end{aligned} \tag{34}$$

$$\begin{aligned} \Gamma_t^{(1)} = {} & \frac{\Gamma_{xx}^{(1)}}{\mathrm{Pe}} + \frac{\Gamma^{(1)}(-k^2)}{\mathrm{Pe}} + \left[h^{(0)}h^{(1)}\Gamma^{(0)}(-Ch_{xxx}^{(0)}) + \frac{h^{(0)2}}{2}\Gamma^{(1)}(-Ch_{xxx}^{(0)}) \right. \\ & + \frac{h^{(0)2}}{2}\Gamma^{(0)}(-Ch_{xxx}^{(1)}) + \frac{h^{(0)2}}{2}\Gamma^{(0)}(Ch_x^{(1)}k^2) + h^{(1)}\Gamma^{(0)}\Gamma_x^{(0)} + h^{(0)}\Gamma^{(1)}\Gamma_x^{(0)} \\ & \left. + h^{(0)}\Gamma^{(0)}\Gamma_x^{(1)} - h^{(0)}h^{(1)}\Gamma^{(0)}G\sin\theta - \frac{h^{(0)2}}{2}\Gamma^{(1)}G\sin\theta \right]_x - \frac{h^{(0)2}}{2}\Gamma^{(0)}Ch^{(1)}k^4 \\ & + \frac{h^{(0)2}}{2}\Gamma^{(0)}Ch_{xx}^{(1)}k^2 - h^{(0)}\Gamma^{(0)}\Gamma^{(1)}k^2. \end{aligned} \tag{35}$$

The spatially and temporally evolving base states for this problem, given by (17) and (18), preclude a simple normal-mode eigenvalue analysis. We therefore conduct a transient-growth analysis (TGA) of the evolving base states which relies on the concept of 'momentary stability' as a measure of instantaneous stability of a time-dependent base flow [26–28].

To elucidate this approach we define the "energy" of a disturbance, E_q, as,

$$E_q(t) \equiv \int_0^\infty (q - q_\infty)^2(x,t)\mathrm{d}x, \tag{36}$$

for which $q = (h^{(0)}, \Gamma^{(0)}, h^{(1)}, \Gamma^{(1)})$ and $q_\infty = (b, 0, 0, 0)$. These, of course, are not physical energies, but simply a measure of growth. We then define amplification ratios for the disturbances in the height and surfactant, $\mathcal{G}_h$ and $\mathcal{G}_\Gamma$, respectively. These represent the ratio of disturbance to base state 'energy' at time t normalized by the initial value:

$$\mathcal{G}_h(t) \equiv \frac{(E_{h^{(1)}}/E_{h^{(0)}})(t)}{(E_{h^{(1)}}/E_{h^{(0)}})(t=0)}, \quad \mathcal{G}_\Gamma(t) \equiv \frac{(E_{\Gamma^{(1)}}/E_{\Gamma^{(0)}})(t)}{(E_{\Gamma^{(1)}}/E_{\Gamma^{(0)}})(t=0)}. \tag{37}$$

To extract further information about the destabilizing mechanism, variables to track the overall instant growth rates are defined. They are given by,

$$\lambda_h(t) = \frac{1}{\mathcal{G}_h}\frac{\mathrm{d}\mathcal{G}_h}{\mathrm{d}t} = \lambda_{h^{(1)}} - \lambda_{h^{(0)}}, \quad \lambda_\Gamma(t) = \frac{1}{\mathcal{G}_\Gamma}\frac{\mathrm{d}\mathcal{G}_\Gamma}{\mathrm{d}t} = \lambda_{\Gamma^{(1)}} - \lambda_{\Gamma^{(0)}}, \tag{38}$$

where the λ terms are defined as, $\lambda_i = \frac{1}{2E_i}\frac{\mathrm{d}E_i}{\mathrm{d}t}$ [26].

2.4. Initial and boundary conditions

The initial and boundary conditions can have a significant influence on the evolution of the film. In the present work, we shall consider the much-studied "constant flux" case, which involves the flow of a film down an incline from an infinite reservoir from which it can draw both fluid and surfactant. Initial conditions that reflect this physical situation are given by:

$$h^{(0)}(x,0) = (1-x^2-b)F(1-x)+b, \tag{39}$$

$$\Gamma^{(0)}(x,0) = F(1-x), \tag{40}$$

where b represents the thickness of the precursor layer, and $F(x) = 1/2[1+\tanh(100x)]$; these initial conditions are shown in Figure 2. The boundary conditions for this situation are set as,

$$h^{(0)}(0,t) = \Gamma^{(0)}(0,t) = 1, \tag{41}$$

$$h^{(0)}_x(x_{\max},t) = h^{(0)}_{xxx}(x_{\max},t) = 0, \tag{42}$$

$$h^{(0)}(x_{\max},t) = b, \quad \Gamma^{(0)}_x(x_{\max},t) = 0, \tag{43}$$

thus pinning both the height and surfactant concentration to fixed values at $x = 0$, which is consistent with the assumed constant flux condition.

The initial conditions for the applied disturbances, $h^{(1)}$ and $\Gamma^{(1)}$, are localized near the origin of the flow and are defined as,

$$h^{(1)}(x,0) = \Gamma^{(1)}(x,0) = \exp(-x^2). \tag{44}$$

Other choices of the initial conditions for $h^{(1)}$ and $\Gamma^{(1)}$ give rise to quantitative rather than qualitative differences in the numerical solutions. Finally, the boundary conditions for $h^{(1)}$ and $\Gamma^{(1)}$ are expressed by:

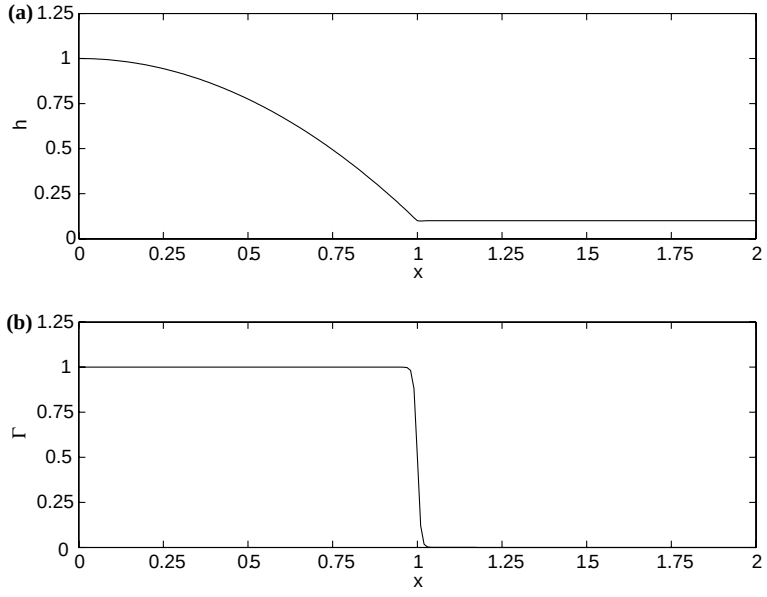

Figure 2. Initial conditions for the (a) film thickness, and (b) surfactant concentration.

$$h_x^{(1)}(0,t) = h_x^{(1)}(x_{\max},t) = 0, \tag{45}$$

$$h_{xxx}^{(1)}(0,t) = h_{xxx}^{(1)}(x_{\max},t) = 0, \tag{46}$$

$$\Gamma_x^{(1)}(0,t) = \Gamma_x^{(1)}(x_{\max},t) = 0. \tag{47}$$

3. Numerical results

In this section, we present a discussion of the numerical results for this system. The results associated with the base state evolution will be presented first, followed by those associated with the TGA. First, however, a brief description of the numerical procedure employed in this study is presented.

3.1. Numerical procedure

Two independent numerical procedures have been used to solve the highly nonlinear coupled system of partial differential equations. One procedure is PDECOL, which uses finite-element collocation in space and Gear's method in time and has been used to solve many related problems [25,26]. The other procedure employs an adaptive method with Petrov-Galerkin projections and Gear's method in time on a non-uniform grid. Identical results were obtained upon comparison of the solutions from these codes. Typically, 2000–3000 grid points were used to carry out the computations on a computational domain of up to $x_{\max} = 50$, with convergence being demonstrated upon mesh refinement.

For this problem the initial and boundary conditions applied are those listed in the previous section. Full numerical results have been obtained for a range of parameter values. The range and scale of all parameters employed in this problem can be found in Table 1. The next section presents a discussion of the results produced over these ranges.

Table 1. Order of magnitude estimates of the relevant parameteric groups.

System Parameter	Units/Representation	Typical Value
ρ	kg m^{-3}	10^3
g	m s^{-2}	10^0
H	m	10^{-4}–10^{-8}
L	m	10^{-2}–10^{-6}
σ_0	N m^{-1}	10^{-2}–10^{-3}
σ_m	N m^{-1}	10^{-2}–10^{-3}
Π	N m^{-1}	10^{-3}–10^{-5}
μ	Pa s	10^{-2}–10^{-4}
D_s	m^2 s^{-1}	10^{-9}–10^{-10}
H_b	m	10^{-5}–10^{-9}
G	$\rho g H L/\Pi$	10^1–10^{-1}
$\mathcal{C}$	$\epsilon^2\sigma_m/\Pi$	10^{-1}–10^{-4}
Pe	$\Pi H/\mu D_s$	10^3–10^5
ϵ	H/L	10^{-2}–10^{-4}

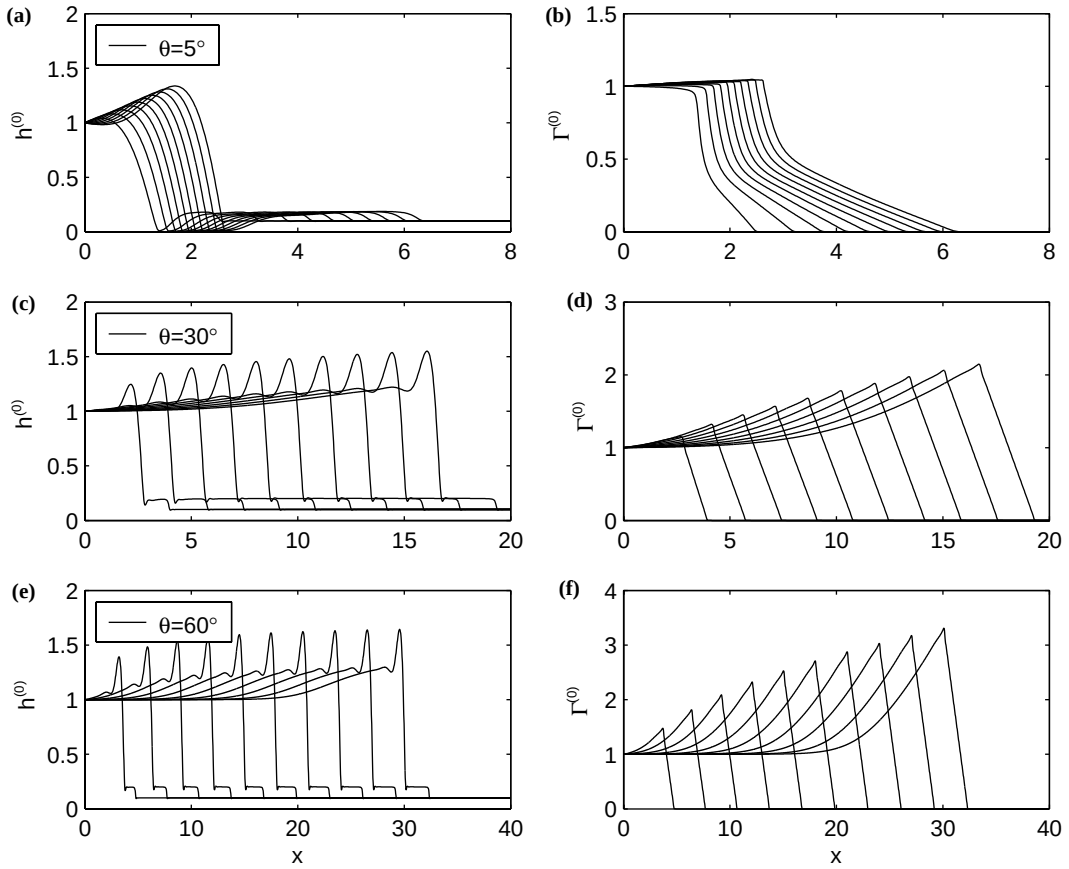

Figure 3. Film thickness and surfactant concentration evolution shown in panels (a), (c), (e), and (b), (d), (f), respectively for $\theta = 5^\circ$, $\theta = 30^\circ$, and $\theta = 60^\circ$ obtained with the parameter set $\mathrm{Pe} = 1000$, $G = 1{\cdot}0$, $C = 0{\cdot}01$, and $b = 0{\cdot}1$ over 100 dimensionless time units.

3.2. Base-state evolution

In Figure 3 we show the effect of varying θ on the evolution of $h^{(0)}$ and $\Gamma^{(0)}$ for $\mathrm{Pe} = 1000$, $G = 1{\cdot}0$, $b = 0{\cdot}1$, and $C = 0{\cdot}01$. Inspection of Figure 3 reveals that at small angles, gravitational forcing is weak and the fluid is driven slowly down the slope; in this case the evolution is reminiscent of a spreading surfactant covered droplet [26], with a structure, resembling a "step", developing at the foot of the main fluid ridge, approximately at the surfactant leading edge. As will be discussed below, this feature of the flow, which is consistently present for all θ values, is produced by the introduction of surfactant and indicates that the surfactant will play an important role at the leading edge of the fluid film. For an inclination angle of 30° the increase in relative significance of gravity gives rise to an accumulation of fluid behind the step and faster spreading rates. At higher angles still, as shown in Figure 3(e), the gravitational driving forces become even more significant, leading to more pronounced fluid ridges formed behind the step; the $h^{(0)}$ profiles rapidly exhibit quasi-steady travelling-wave-like solutions with elevated capillary ridges. An additional structure appears behind the main fluid ridge, forming a weak fluid 'hump' which has been previously observed experimentally [10]. Its formation is driven by a balance of Marangoni forces, which drive flow from high to low surfactant concentrations (that is from the ridge back towards the flow origin), and

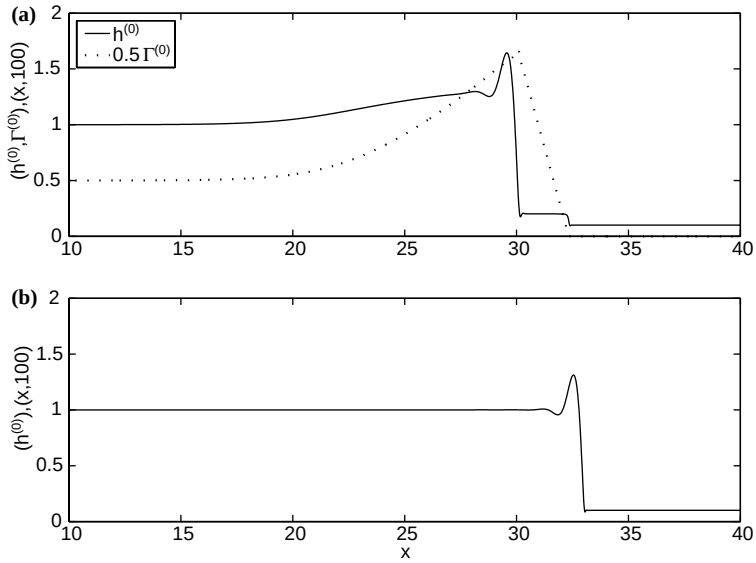

Figure 4. Comparison of the (a) film thickness (solid line) and surfactant concentration (dotted line) for $\theta = 60^\circ$, $\mathrm{Pe} = 1000$, $G = 1{\cdot}0$, $C = 0{\cdot}01$, and (b) the uncontaminated film thickness evolution obtained with $C = 0{\cdot}01$, $b = 0{\cdot}1$, at $t = 100$.

gravity. The structure is seen to exist in Figure 3(c) and (e), but is more clearly present in the comparisons of Figure 4.

The evolution of the surfactant concentration for different θ values is shown in Figures 3(b), (d), and (f). At small θ values the surfactant is drawn down the slope as the fluid spreads. For higher θ values the solutions appear to change resulting in a different type of surfactant concentration profile: a near monotonic increase in $\Gamma^{(0)}$, reaching a maximal value at the propagating fluid ridge, followed by an essentially linear decrease to zero. In all the cases studied, the leading edge of the surfactant concentration profile lies ahead of the main fluid front, coinciding with the region in which the raised step adjusts back onto the undisturbed precursor layer.

To show the interaction between the evolving profiles of $h^{(0)}$ and $\Gamma^{(0)}$ clearly, height and surfactant concentration profiles have been overlayed in Figure 4(a). The features which have been highlighted above immediately become clear. The protruding step coincides with the portion of the surfactant profile over which $\Gamma^{(0)}$ exhibits an essentially linear profile. The Marangoni stresses acting in this region have deformed the underlying film and given rise to the fluid step, this is a common mechanism seen in many works on surfactant spreading [20]. The maximum surfactant concentration coincides approximately with the steepest part of the main fluid ridge and in turn produces a second concentration gradient which acts up the slope towards the flow origin. The balance between this gradient and the gravitational forces acting in the opposite direction leads to fluid accumulation and the formation of a hump on the upstream side of the main fluid ridge.

Next, we contrast the structures shown in Figure 4(a) with those associated with the uncontaminated case in order to highlight the qualitative changes in the flow profiles arising from the inclusion of surfactant. In Figure 4(b), we plot $h^{(0)}$ for the surfactant free case; this profile was obtained by setting $\Gamma^{(0)} = 0$ and rescaling the problem. Close inspection of panels (a) and (b) in Figure 4 reveals that the flow of the uncontaminated film is characterized

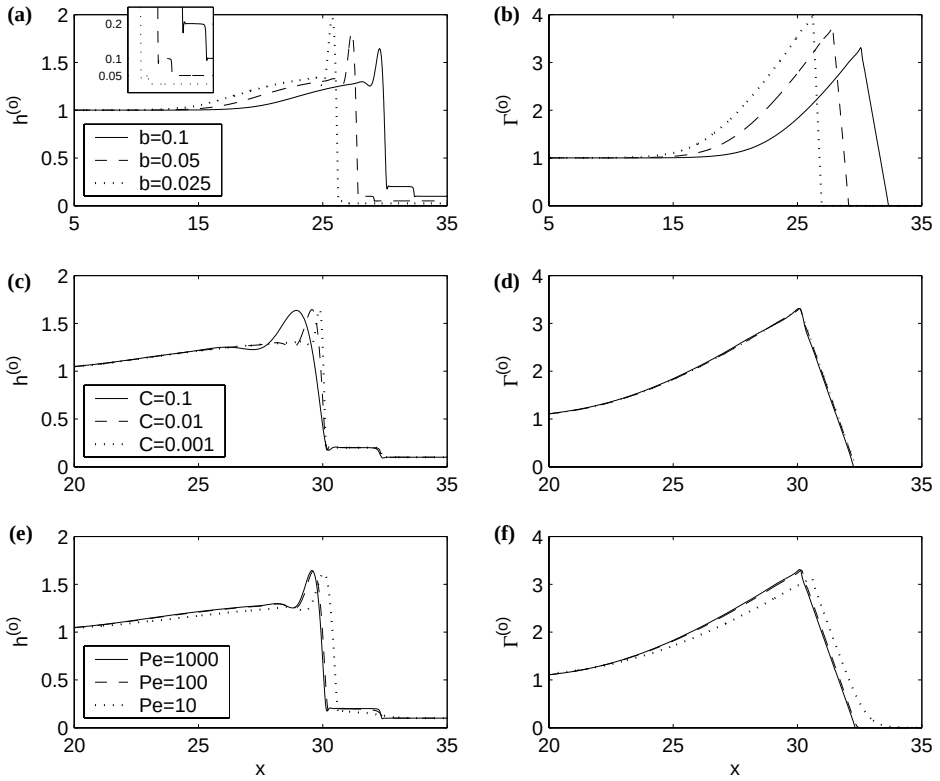

Figure 5. The effect of varying b, C and, Pe on $h^{(0)}$ and $\Gamma^{(0)}$ shown in panels (a), (c), (e) and (b), (d), (f), respectively. Unless otherwise stated in the legend, the parameters are $\theta = 60^{\circ}$, $\mathrm{Pe} = 1000$, $G = 1{\cdot}0$, $C = 0{\cdot}01$, $b = 0{\cdot}1$, at $t = 100$.

by the formation of a travelling-wave solution [13]. Note in particular from Figure 4(b) the absence of the "step" and the "hump" structure with its long tail shown in Figure 4(a).

We also investigate the effect of varying b, C and Pe on the flow profiles. In panels (a) and (b) of Figure 5, it can be seen that for smaller values of b, the evolution of the fluid front is retarded leading to the formation of larger capillary ridges while reducing the scale of the protruding fluid step (the inset in panel (a) highlights the reduction of this structure). These effects are made clearer in the concentration profiles, as they exhibit a reduced lateral extent and an increasing maximum value as b decreases. In panels (c) and (d) changes in C are investigated. In this situation a reduction in surface tension allows sharper fluid fronts to form. However, this has virtually no effect on either the position and structure of the step or on the evolution of the surfactant concentration profile. In panels (e) and (f) the effect of variation of Pe is shown. As this parameter decreases the relative effect of surface diffusion is increased. This leads to greater spreading of the surfactant and a reduction in the surfactant concentration gradients formed. This produces smaller step and hump structures, and apparently leads to faster spreading.

As with other cases of flow on an inclined plane the solutions obtained form travelling wave patterns that can be easily dealt with through translation into a moving frame of reference [9]. Thus to conclude this section, we closely examine the step structure and the speed of the flow by comparing the numerical solutions to the predictions made earlier in Section 2.2. In Figure 6 we show comparisons of the speed, height and surfactant-concentration gradient

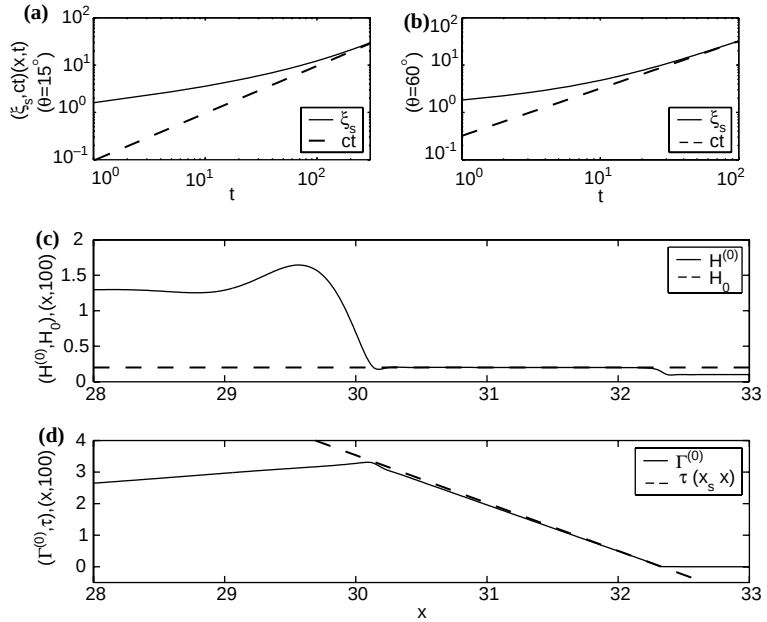

Figure 6. Comparison of travelling wave predictions to the results obtained through numerical simulation. Panels (a) and (b) compare step speed for $\theta = 15^\circ$ and 60°, respectively, while step height and surfactant concentration gradient comparisons are made in panels (c) and (d), respectively. Unless otherwise stated in the legend, the parameters are $\theta = 60^\circ$, Pe = 1000, $G = 1{\cdot}0$, $C = 0{\cdot}01$, $b = 0{\cdot}1$, at $t = 100$.

localized about the step structure; here (26), (32) and (33) are used. In Figure 6 panels (a) and (b) the position of the leading edge of the step is compared to the predicted travelling wave speed. For both large and small angles, the predictions compare well, with higher angle solutions converging faster to the travelling-wave predictions. In the region of the step, both the film height and surfactant concentration gradient show excellent agreement between the analytical prediction and numerical solution.

3.3. Transient-growth analysis

We now turn our attention to the examination of the base-state stability. Figure 7 shows the effect of varying θ on the amplification ratios, $\mathcal{G}_h$ and $\mathcal{G}_\Gamma$, for Pe = 1000, $G = 1{\cdot}0$, $C = 0{\cdot}01$, $b = 0{\cdot}1$ and different k values. Inspection of these results shows that the range of unstable wavenumbers widens with increasing angle of inclination. This change also increases the value of the most unstable wavenumber, which is qualitatively consistent with previous work involving films which exhibit a fingering instability: the finger width decreases (that is, the instability is enhanced) with increasing θ [10]. The range of unstable wavenumbers was found to be restricted to the range, $0 \leq k < 5$, for all parameters considered in the present work.

Having identified that unstable "modes" exist, we deem it important to identify the region that this instability will target as evolution progresses. Figure 8 shows the evolution of $h^{(0)}$ and $\Gamma^{(0)}$ together with those of the disturbances $h^{(1)}$ and $\Gamma^{(1)}$, for $k = 3$ (an estimate of the most dangerous "mode" wavenumber). As shown in panels (a) and (b) both $h^{(1)}$ and $\Gamma^{(1)}$ exhibit highly localized structures, which appear to target the region immediately downstream of the capillary ridge and the maximal surfactant concentration, respectively. It should be noted that the advancing fluid "step" is not targeted by the instability for any of

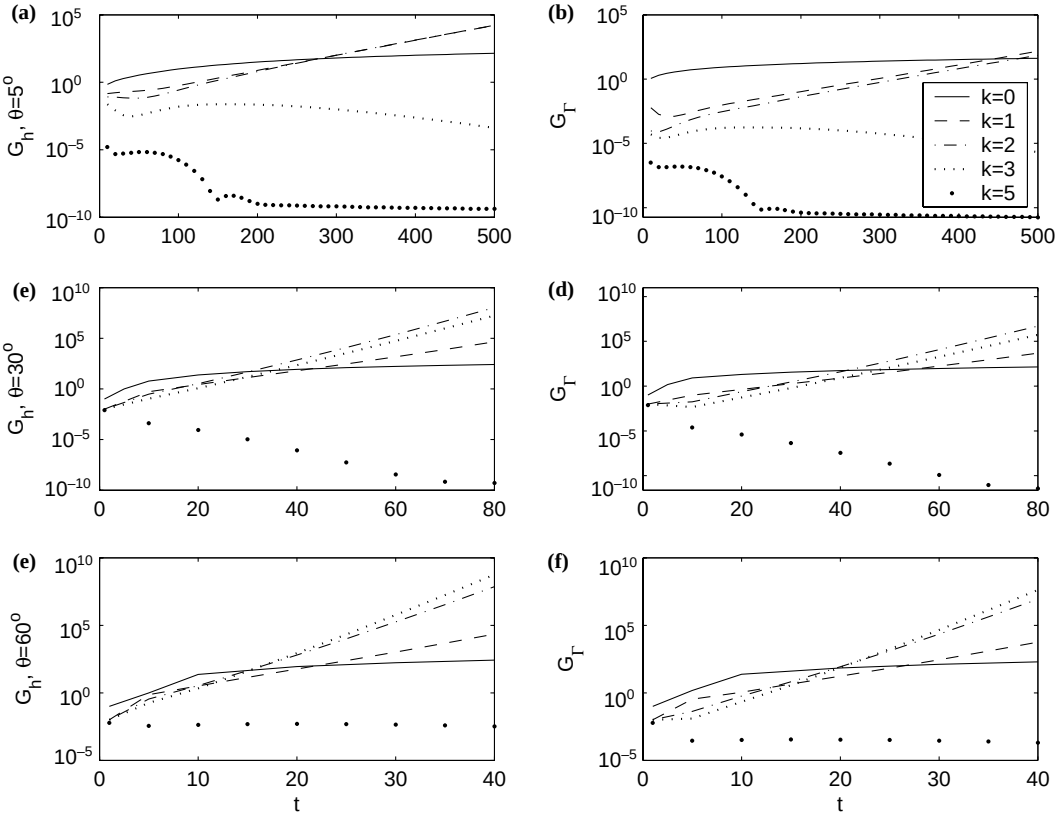

Figure 7. Variation of the amplification ratios, $\mathcal{G}_h$ and $\mathcal{G}_\Gamma$, with θ, for disturbances of different k; the rest of the parameter values are Pe = 1000, $G = 1{\cdot}0$, $C = 0{\cdot}01$, and $b = 0{\cdot}1$.

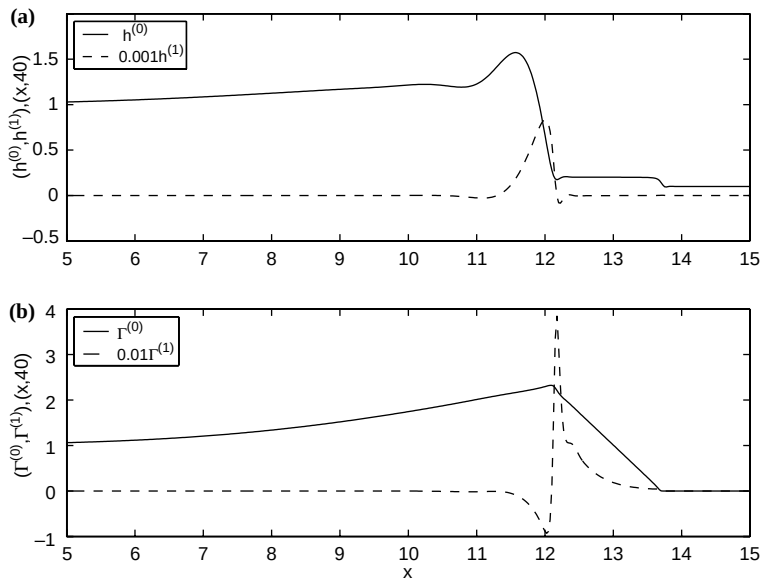

Figure 8. Plots of $h^{(0)}$, $\Gamma^{(0)}$, $h^{(1)}$, and $\Gamma^{(1)}$ for $k = 3$, $\theta = 60^\circ$, Pe = 1000, $G = 1{\cdot}0$, $C = 0{\cdot}01$ and $b = 0{\cdot}1$ shown at $t = 40$.

the parameter values examined. These results suggest that the mobility mechanism normally proposed for the uncontaminated film instability [29] may still be in operation, however, this does not elucidate the role of the surfactant in the present flow. This issue is discussed next.

Using the detailed TGA profiles, Figure 8, we can see that the surfactant disturbances have an inverse response to those exhibited in the fluid height ($h^{(1)}\Gamma^{(1)} < 0$). Thus, the standard fluid-mobility argument, proposing that areas of increased fluid height flow faster, is reinforced as thicker regions will also be relatively deficient in surfactant, producing transient Marangoni stresses that will increase the local thickness further, thereby increasing the relative mobility advantage and destabilizing the flow.

Further information about instability mechanisms can be obtained by decomposing the overall instantaneous growth rates, given by Equation (40), into their component parts. Presenting these terms over a range of angles allows the main destabilizing forces for different cases to be identified; this is shown in Figure 9 wherein only λ_h was considered. For a horizontal substrate, flow destabilization is induced by Marangoni stresses. The insert in panel (a) shows that the gravitational terms are zero-valued, while Marangoni terms destabilize the system (taking positive values) even at long times. Capillary forces tend to stabilize the system (taking negative values), but are smaller than the Marangoni terms leading to instability. As the angle of inclination increases, the gravitational force begins to dominate, yielding the largest destabilizing contribution. The Marangoni stresses continue to provide an additional destabilizing forces while capillary influences remain stabilizing. It should also be noted that inclusion of surfactant effects produces instability in situations wherein the flow would otherwise have been stable in the surfactant-free case [9].

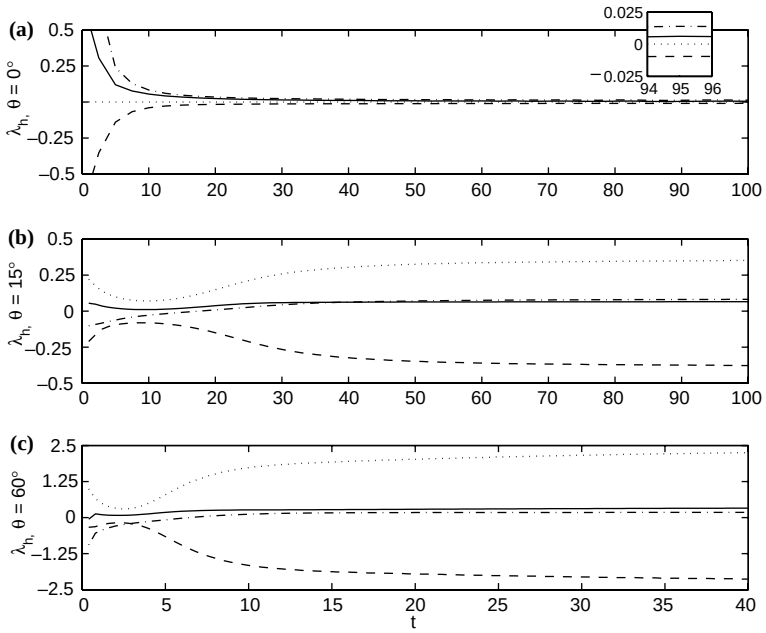

Figure 9. Temporal evolution of the instantaneous growth rate, λ_h for (a) 0°; (b) 15°; and (c) 60° for $k = 2$. The rest of the parameters remain unchanged from Figure 8. In each panel the total growth rate (solid lines), capillary contribution (dashed line), Marangoni contribution (dot-dashed line), and gravitational contribution (dotted line) are shown. The insert in panel (a) presents an enlarged view of the long time behaviour, highlighting the sign and scale of each contribution.

4. Conclusions

The evolution of a gravitationally-driven thin film on an inclined substrate has been examined in the presence of an insoluble surfactant of low concentration under conditions of constant flux. A coupled system of two-dimensional (2-D) nonlinear evolution equations for the film thickness and surfactant concentration was derived using the lubrication approximation. The contact-line singularity was relieved using a precursor layer model. This study extends previous work involving driven uncontaminated films, which exhibit a fingering instability, to account for surfactant-induced effects.

The evolution of the base state film thickness and surfactant concentration, obtained via numerical solutions of the one-dimensional version of the governing equations, was studied. Inspection of these results revealed the formation of a capillary ridge, flanked by a Marangoni driven fluid "step" downstream, and an additional fluid "hump" upstream. At larger inclination angles the film height forms a travelling-wave-like solution. For these cases the surfactant concentration was found to exhibit a monotonic increase from the origin of flow reaching a maximum value at the capillary ridge, followed by an essentially linear decrease over the step region. At lower inclination angles the solution appeared to be similar to those obtained in work on spreading surfactant droplets on horizontal substrates.

The stability of the film evolution was also examined using a transient growth analysis. These results suggest that the film is linearly unstable to transverse disturbances with maximum growth obtained at intermediate wavenumbers. As the inclination of the plate increases, the range of wavenumbers associated with growing perturbations widens. Inspection of the flow profiles reveals that the perturbations in both the film height and surfactant concentration target very specific regions, that coincide approximately with the leading edge of the main fluid ridge and the location of the maximum surfactant concentration, respectively. The introduction of Marangoni stresses was shown to produce instability in cases where gravitationally-driven surfactant-free films would have been stable.

Future work will focus on alternative flow configurations and on obtaining numerical solutions of the fully nonlinear 2-D governing equations. The extension of the present work to account for surfactant solubility is also underway.

Acknowledgements

The authors would like to thank M. R. E. Warner for his helpful thoughts and comments as well as the EPSRC for their support of B. D. E. through a doctoral training account studentship. The authors would also like to acknowledge insightful comments made by the anonymous referees on an earlier version of this paper.

References

1. A. Oron, S.H. Davis and S.G. Bankoff, Long-scale evolution of thin liquid films. *Rev. Modern Phys.* 69 (1997) 931–980.
2. O.K. Matar and S.M. Troian, Linear stability analysis of an insoluble surfactant monolayer spreading on a thin liquid film. *Phys. Fluids A* 9 (1997) 3645–3657.
3. O.K. Matar and S.M. Troian, Spreading of surfactant monolayer on thin liquid film: Onset and evolution of digitated structures. *Chaos* 9 (1999) 141–153.
4. O.K. Matar and S.M. Troian, The development of transient fingering patterns during the spreading of surfactant coated films. *Phys. Fluids* 11 (1999) 3232–3246.
5. H. Huppert, Flow and instability of a viscous current down a slope. *Nature (London)* 300 (1982) 427–429.

6. N. Silva and E.B. Dussan, On the rewetting of an inclined solid surface by a liquid. *Phys. Fluids* 28 (1985) 5–7.
7. S.M. Troian, E. Herbolzheimer, S.A. Safran and J.F. Joanny, Fingering instabilities of driven spreading films. *Europhys. Lett.* 10 (1989) 25–30.
8. R. Goodwin and G.M. Homsy, Viscous flow down a slope in the vicinity of a contact line. *Phys. Fluids A* 3 (1991) 515–528.
9. A.L. Bertozzi and M.P. Brenner, Linear stability and transient growth in driven contact lines. *Phys. Fluids* 9 (1997) 530–539.
10. M.F.G. Johnson, R.A. Schluter, M.J. Miksis and S.G. Bankoff, Experimental study of rivulet formation on an inclined plate by fluorescent imaging. *J. Fluid Mech.* 394 (1999) 339–354.
11. Y. Ye, and H-C. Chang, A spectral theory for fingering on a prewetted plane. *Phys. Fluids* 11 (1999) 2494–2515.
12. M.H. Eres, L.W. Schwartz and R.V. Roy, Fingering phenomena for driven coating films. *Phys. Fluids* 12 (2000) 1278–1295.
13. L. Kondic and J. Diez, Pattern formation in the flow of thin films down an incline: Constant flux configuration. *Phys. Fluids* 13 (2001) 3168–3184.
14. L. Kondic and J. Diez, Flow on films with patterned surfaces: Controlling the instability. *Phys. Rev. E* 65 (2002) 045301:1–4.
15. L. Kondic and J. Diez, Flow of thin films on patterned surfaces. *Colloids Surf. A* 214 (2003) 1–11.
16. L.W. Schwartz, R.A. Cairncross and D.E. Weidner, Anomalous behaviour during leveling of thin coating layers with surfactant. *Phys. Fluids* 8 (1996) 1693–1695.
17. M.S. Borgas and J.B. Grotberg, Monolayer flow on a thin film. *J. Fluid Mech.* 193 (1988) 151–170.
18. D.P. Gaver III and J.B. Grotberg, The dynamics of a localized surfactant on a thin film. *J. Fluid Mech.* 213 (1990) 127–148.
19. D.P. Gaver III and J.B. Grotberg, Droplet spreading on a thin viscous film. *J. Fluid Mech.* 235 (1992) 399–414.
20. O.E. Jensen and J.B. Grotberg, Insoluble surfactant spreading on a thin viscous film: shock evolution and film rupture. *J. Fluid Mech.* 240 (1992) 259–288.
21. D. Halpern and J.B. Grotberg, Dynamics and transport of a localised soluble surfactant on a thin film. *J. Fluid Mech.* 237 (1992) 1–11.
22. O.E. Jensen and J.B. Grotberg, The spreading of heat or soluble surfactant along a thin liquid film. *Phys. Fluids* 5 (1993) 58–68.
23. O.E. Jensen, D. Halpern and J.B. Grotberg, Transport of passive solute by surfactant-driven flows. *Chem. Engng. Sci.* 49 (1994) 1107–1117.
24. Y.L. Zhang, O.K. Matar and R.V. Craster, A theoretical study of chemical delivery within the lung using exogenous surfactant. *Med. Engng. Phys.* 25 (2002) 115–132.
25. M.R.E. Warner, R.V. Craster and O.K. Matar, Unstable van der Waals driven line rupture in Marangoni driven thin viscous films. *Phys. Fluids* 14 (2002) 1642–1654.
26. M.R.E. Warner, R.V. Craster and O.K. Matar, Fingering phenomena associated with insoluble surfactant spreading on thin liquid films. *J. Fluid Mech.* 510 (2004) 169–200.
27. B.J. Fischer and S.M. Troian, Thinning and disturbance growth in liquid films mobilized by continuous surfactant delivery, *Phys. Fluids* 15 (2003) 3837–3845.
28. B.J. Fischer and S.M. Troian, Growth and decay of localized disturbances at the leading edge of a surfactant monolayer spreading on a thin viscous film. *Phys. Rev. E* 67 (2003) 016309:1–11.
29. M.A. Spaid and G.M. Homsy, Stability of Newtonian and viscoelastic dynamic contact lines. *Phys. Fluids* 8 (1996) 460–478.